The International Journal of Advanced Manufacturing Technology (2022) 119:1283–1300
https://doi.org/10.1007/s00170-021-08225-6

APPLICATION

Numerical simulation and optimization of fine-blanking process for copper alloy sheet

Chun-Chih Kuo[1,2] · Kuo-Wang Liu[1] · Tse-Chang Li[2] · Dai-You Wu[1] · Bor-Tsuen Lin[1,2]

Received: 22 February 2021 / Accepted: 14 October 2021 / Published online: 10 November 2021

Abstract
When the fine-blanking process is used, secondary grinding or processing can be omitted because the shear surface of fine-blanking parts can achieve almost zero fracture zone requirements. The primary objective of the fine-blanking process is to reduce the fracture zone depth and die roll zone width. This study used a 2.5-mm-thick central processing unit (CPU) thermal heat spreader as an example. Finite element analysis software was employed to simulate and optimize the main eight process parameters that affect the fracture zone depth and die roll zone width after fine-blanking: the V-ring shape angle, V-ring height of the blank holder, V-ring height of the cavity, V-ring position, blank holder force, counter punch force, die clearance, and blanking velocity. Simulation analysis was conducted using the L_{18} ($2^1 \times 3^7$) Taguchi orthogonal array experimental combination. The simulation results of the fracture zone depth and die roll zone width were optimized and analyzed as quality objectives using Taguchi's smaller-the-better design. The analysis results revealed that with fracture zone depth as the quality objective, 0.164 mm was the optimal value, and counter punch force made the largest contribution of 25.89%. In addition, with die roll zone width as the quality objective, the optimal value was 1.274 mm, and V-ring height of the cavity made the largest contribution of 29.45%. Subsequently, this study selected fracture zone depth and die roll zone width as multicriteria quality objectives and used the robust multicriteria optimal approach and Pareto-optimal solutions to perform multicriteria optimization analysis. The results met the industry's fraction zone depth standard (below 12% of blank thickness) and achieved a smaller die roll zone width.

Keywords Fine-blanking · Finite element analysis · Multicriteria optimization · Pareto-optimal

1 Introduction

The difference between traditional blanking and the fine-blanking process is that fine-blanking is a precise manufacturing process, no post-processing, and better efficiency and cost thanks to smaller die clearance and higher blanking quality than traditional processes. Fine-blanking process is widely used in aerospace and automobile production.

Thipprakmas et al. [1] improved the fine-blanking process by predicting the V-ring indenter's geometric parameter optimization and influence using finite element analysis, Taguchi method, and ANOVA. Yin et al. [2] created a mathematical life model for fine-blanking die using backpropagation neural network to gain the inner law and behavior between die wear and working parameters, thereby enabling wear prediction for fine-blanking die. Liu et al. [3] used finite element analysis and experiment to improve fractures that occurred to complex parts during the fine-blanking process, which mainly focused on the effects of surface quality by the angle of nearby edges, the height of ridges, and parametric designing methods for complex parts. Wang et al. [4] proposed a new blanking method by replacing V-ring indenter using slot structure, which creates high hydrostatic stress, to improve tearing; the proposed method creates a buffed surface along almost full blank thickness, eliminating most tearing effects. Liu et al. [5] proposed an optimization analysis which consists of minimizing die roll dimensions, an indenter mechanism set on cutting edge, and finite element analysis to

✉ Bor-Tsuen Lin
bt_lin@nkust.edu.tw

[1] Department of Mechatronics Engineering, National Kaohsiung University of Science and Technology (First Campus), Kaohsiung, Taiwan

[2] Metal Product Development Technology R&D Center, National Kaohsiung University of Science and Technology (First Campus), Kaohsiung, Taiwan

validate the optimization; the study shows the optimized fine-blanking die can limit blanking deformation and the increase of die roll. Zheng et al. [6] discussed the effects of die roll dimension for evaluating product quality due to changes to product shape and material, the evolution of blank holder structure, and blanking press, which acts as a crucial part of fine-blanking process quality control in electric automotive industries. Karbaukh et al. [7] proposed the multiple different wedge-shaped knives for rolled-stock cutting equipment and process, which converted deformation energy from machine frame and drive into hydraulic press, namely, a stress concentrator for effective cutting work. Sahli et al. [8] proposed an optimization process for cold-rolled steel cutting, which consists of parameters such as burr condition, cutting edge appearance, and dimension, using the numerical analysis method.

In the fine-blanking process, the directions of blanking and shearing are related to the anisotropic mechanical properties of the metal blank and orientation of crystallites. According to observations of the side microstructure in fine-blanking products, the blanking and shearing directions can be divided into the deformation, shear, and failure zones. The current fine-blanking process tends to reduce the size of the deformation zone and improve the initiation and growth of microcracks in the failure zone. The literature has mostly discussed the application of FEA combined with a damage model to simulate the damage behavior of the shear plane [9] and die design to control the quality of the shear surface [10]. Zhao et al. [11] conducted microstructure observation to determine the fracture failure mode in the shear zone of the DP600 steel plate fine-blanking process. A self-adjustable triaxial stress model was adopted to simulate the damage behavior of the shear zone. Wang et al. [12] used a scanning electron microscope to observe the microstructure of the shear surface of an ultra-thin blank and employed the Abaqus software package to simulate a three-dimensional fine-blanking process on the basis of effective plastic strain and the Gurson–Tvergaard–Needleman shear correction model. In addition, Barik et al. [13] used Simulation software ABAQUS to change the forming and geometric parameters to perform FEA on the fine-blanking process of aluminum alloy AA6082-T6. An experimental design method was employed to optimize the fine-blanking process and the effect of forming and geometric parameters on burr formation on the metal blank after fine-blanking. This method can improve product quality and reduce production costs. Tanaka et al. [14] used FEA to calculate the ratio of the shear plane to the fracture surface and evaluated the ductile fracture criteria of Oyane, Cockcroft, and Latham using four punching methods. The results indicated that various types of shear surface will be affected by the clearance between the punch and die, clamping method of the blank, and selection of ductile fracture criteria.

A servo die cushion is a forming method that can self-adjust the blank holder force in the press equipment with high speed and stability. The servo press exhibits an adjustable curvilinear motion on the upper press, and the servo die cushion can adjust the blank holder force arbitrarily. Therefore, blanking processes that cannot be formed by conventional machinery or hydraulic presses can be achieved according to the forming conditions required by different blanking processes. At present, literature on servo die cushions involve servomotor-related technology and metal-forming industry applications [15], the use of high-frequency impulsive vibration to improve forming quality and efficiency [16], and the use of FEA and remeshing to define the standard in blanking formability analysis [17]. Kim et al. [18] proposed computer-aided engineering analysis combined with an experimental design method to confirm the technical methods required by the servo press in the forging process. The experimental design method could effectively optimize the pressure distribution required for the forming process of continuously variable pulleys and spur gears. Olguner and Bozdana [19] proposed a finite element model for a dual-phase steel plate to evaluate the reduction of steel plate thickness and the change of forming load in the pulse pressure distribution curve during the drawing process. They also changed the frequency and amplitude of the pulse pressure to perform elastoplastic FEA with DEFORM-3D. Fallahiarezoodar et al. [20] applied a servo die cushion to the drawing and formation of the U-channel of Al 5182-O. A blank was stretched and bent when it was near the rounded corner of the cavity; it was not bent when it passed the rounded corner. The reversing load generated by the bending process produced a residual stress distribution in the direction of the blank section. The application of the servo die cushion reduced the residual stress distribution and wall springback. Moreover, Esmaeilpour et al. [21] used a servo press and die cushion to form three aluminum alloy sheets in a cross shape. The uniaxial tensile test was used to construct the anisotropic properties of the aluminum alloy sheet, and the Argus system was used to measure the strain of the draw forming. The formed part was cut in two different directions using a water-jet machine to measure the thickness change after forming. The study used Yld2000-2D and Hill's 48 yield function for numerical simulation analysis and comparison with experimental values.

The most common problem encountered in the process of blanking products is how to reduce costs and improve quality, which is generally related to the selection of process parameters, die geometry, and blank material. In the industry, the trial and error method is often used for tryout process, but this relies on rich experience and involves huge costs, and discovering

solutions for nonlinear problems could be difficult. In the blanking process, the fracture zone and die roll zone are the surface features that must be produced on the shear surface. Both zones will affect the size and performance of the finished product and even cause problems such as secondary processing. Therefore, the ability to control the size of the fracture and die roll zones in the blanking process is crucial.

The present study used a thickness 2.5 mm C1100 copper plate central processing unit (CPU) thermal heat spreader as an example; the relevant dimensions is shown in Fig. 1, to investigate the key process parameters of fine-blanking, including the effects of blanking velocity, V-ring height of the blank holder, V-ring height of the cavity, V-ring shape angle, V-ring position, blank holder force, counter punch force, and die clearance on the fracture zone depth and die roll zone width. First, this study performed a tensile test simulation analysis on the C1100 copper plate and imported the test parameters into the DEFORM software package to obtain the critical damage value of the material. Subsequently, the Taguchi orthogonal array L_{18} ($2^1 \times 3^7$) experiment combination was used to conduct a fine-blanking simulation analysis. Moreover, the fracture zone depth and die roll zone width were set as the quality objectives for process optimization analysis, where the Taguchi method's smaller-the-better quality design was used to identify the correlation between process parameters and quality objectives through ANOVA. Furthermore, the optimal combination of process parameters was obtained through the robust multicriteria optimal approach and Pareto-optimal solutions. Finally, experiments were performed to verify the accuracy of the results of the optimal process parameter combination analysis.

2 Experimental equipment and die

The greatest differences between a fine-blanking die and a general blanking die are the die clearance, V-ring, and counter punch in the cavity. The die clearance is approximately 0.5–1.5% of the blank thickness, and the shear surface of the finished product occupies more than 80% of the shear surface. V-rings are commonly added to the blanks and cavities to increase the precompression internal stress of the blanks for reducing the generation of tensile stress, thereby improving the plasticity of the material, slowing the generation of the fracture zone, and preventing blanks in the waste area from flowing into the finished product area. The function of the counter punch in the cavity is to press the material on the back during shearing, mainly to increase the precompression internal stress inside it to increase its plasticity and restrain the material to ensure greater flatness.

The fine-blanking process is divided into three stages, as depicted in Fig. 2. Before blanking, the blank is clamped and fixed by the blank holder and the cavity, the punch descends, and the counter punch contacts the blank simultaneously. During blanking, the counter punch exerts ejection force to clamp the material and perform the blanking while pressing the punch into the cavity. After blanking, the counter punch continues to support the material and stops at the end position after the punch is pressed into the cavity and exceeds the thickness of the blank. After the punch rises and is demolded, the blank is pushed out of the cavity to complete the fine-blanking process. The aforementioned actions of the counter punch can be completed by a servo die cushion.

To meet practical requirements, a fine-blanking die was designed with the CPU thermal heat spreader parts as an example. The die structure is presented in Fig. 3. The upper die system included an upper die set,

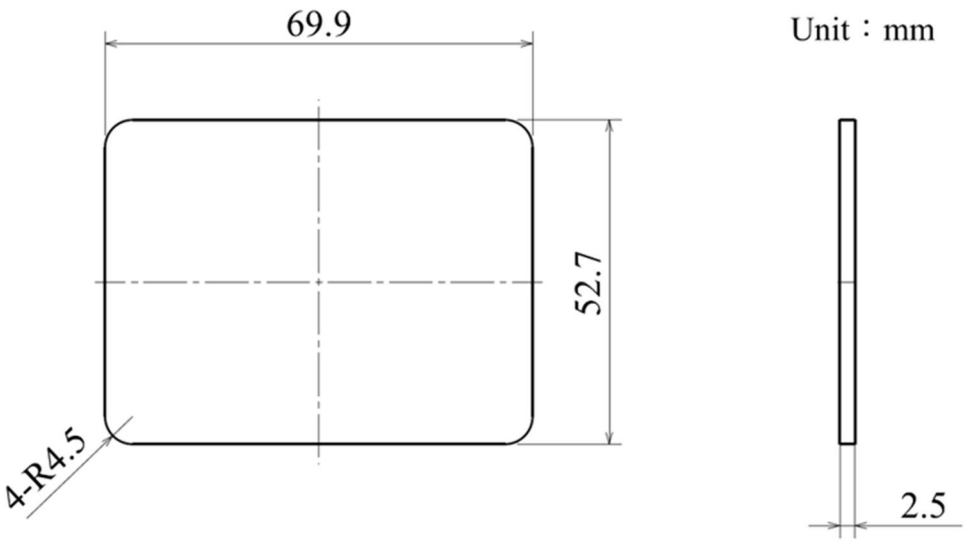

Fig. 1 Dimensions of the CPU thermal heat spreader carrier

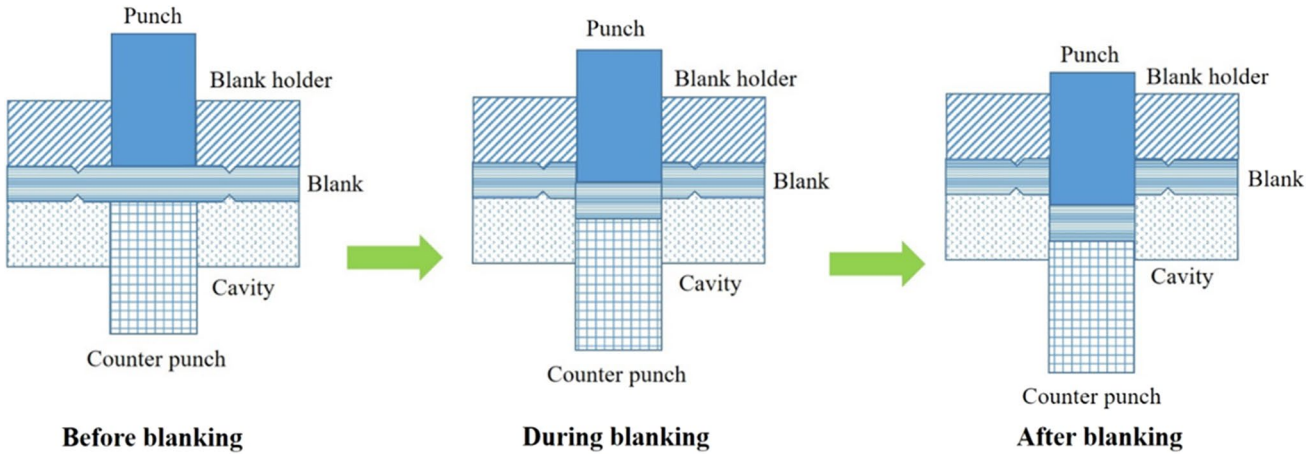

Fig. 2 Fine-blanking process

upper block, upper die base, nitrogen gas spring, punch, punch fix plate, punch back plate, blank holder plate, holder back plate, and guide post. The lower die system included a lower die set, lower die base, counter punch, servo cushion block, cavity insert, cavity plate, cavity back plate, and bushing. First, the blank was placed on the cavity plate for positioning. During blanking, the blank was clamped by the blank holder through the force exerted by the nitrogen gas spring. The blank was pressed into the cavity simultaneously by the punch, and the counter punch in the cavity was pressed against the blank by the servo die cushion to generate an ejection force. In cooperation with the servo die cushion, the die was sheared from top to bottom. Upon completion, the upper die system opened, the finished blank was ejected from the cavity by the counter punch, and the blank could be removed. The thickness 2.5 mm C1100 copper plate was 99.9% copper. The blank was 60 mm long × 70 mm wide. In addition, this study used a servo press (SEYI SD1-200, Shieh Yih Machinery Industry, Taiwan) for the fine-blanking experiments, as depicted in Fig. 4. The forming tonnage of the servo press was 200 ton, the maximum output tonnage of the servo die cushion was 15 ton, and the maximum forming speed was 50 strokes/min. The forming motion curves can be set according to different forming requirements, and the servo die cushion can be matched with said motion to directly control the stroke and speed.

Fig. 3 Fine-blanking die

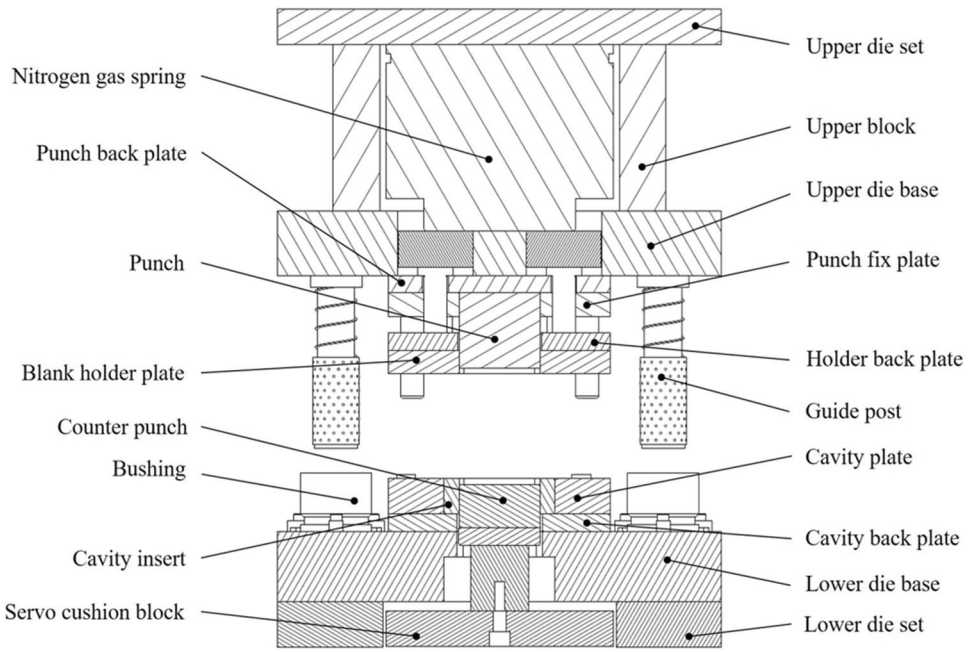

Fig. 4 Servo press

3 Tensile test

In the simulation analysis, a tensile test had to be conducted to obtain the mechanical properties of the copper alloy C1100. The size of the tensile test piece conformed to ASTM E8M specifications, and the size and test piece are presented in Fig. 5. This study used a 100 kN MTS 810 dynamic tensile testing machine to measure the mechanical properties of the copper alloy C1100. The tensile speed of the tensile test was 1 mm/min. The tensile test could only obtain the load–elongation curve, whereas the true stress and true strain were based on the actual cross-sectional area and length of the test piece under the load. Therefore, the load–elongation curve of the material had to be converted into a true stress–true strain curve. The converted maximum true stress and true strain of the material are 352MPa and 0.42, respectively. The fitting curve is stretched to 1.0 in strain for illustrating the failure of high-formability material. The Ludwik hardening law is used for fitting true stress–strain curves after necking. Figure 6 depicts the true stress (σ)–true strain (ε) curve of the copper alloy C1100. The curve fitting formula is shown as follows:

$$\sigma = 79.28 + 526.69\varepsilon^{0.72} \tag{1}$$

To present a blank fracture situation during shearing, ductile fracture criteria must be used as the basis for the blank fracture during the simulation analysis. This study used the normalized Cockcroft–Latham fracture criterion [25] as the critical damage value in simulation analysis. The formula is shown as follows:

$$C = \int_0^{\overline{\varepsilon_f}} \frac{\sigma^*}{\overline{\sigma}} d\overline{\varepsilon} \tag{2}$$

where C represents failure value, $\overline{\varepsilon}_f$ represents equivalent strain when deforming, $\overline{\sigma}$ represents equivalent stress, and σ^* represents maximum primary stress. The formula above calculates the maximum failure value by integrating ratios of the material's primary and equivalent stress with equivalent strain. Failure occurs to the material as soon as the energy function of unit volume reaches the limit. Verification of failure value is done by comparing simulation and experiment of the tensile stress test and fine-blanking process [25]. Consistency is shown in both the tensile stress test and the fine-blanking process [26, 27]. Therefore, to obtain the critical damage value of the copper alloy C1100, the thickness of the material at the necking fracture of the test piece was measured after the tensile test was completed, and then the material tensile test simulation analysis was performed. The analysis model of the tensile test is illustrated in Fig. 7. This study simulated the thickness at the necking fracture to obtain the normalized Cockcroft–Latham critical damage value required by the material, as demonstrated in Fig. 8. The critical damage value of copper alloy in the C1100 tensile test analysis simulation was 2.04. Finally, the obtained mechanical properties of the material were incorporated into DEFORM 2D and DEFORM 3D software for simulation analysis. The load–elongation figure of simulation and experiment, shown in Fig. 9, proves similar results.

4 Optimization of fine-blanking parameters

This study employed the fracture zone depth and die roll zone width of the CPU thermal heat spreader as the quality objectives, as illustrated in Fig. 10. The fracture zone depth was required to be as small as possible to obtain satisfactory size tolerance and avoid secondary processing problems. In addition, to avoid the reduction of the contact area of the finished product, which leads to a poor heat dissipation effect, the die roll zone width had to be as small as possible.

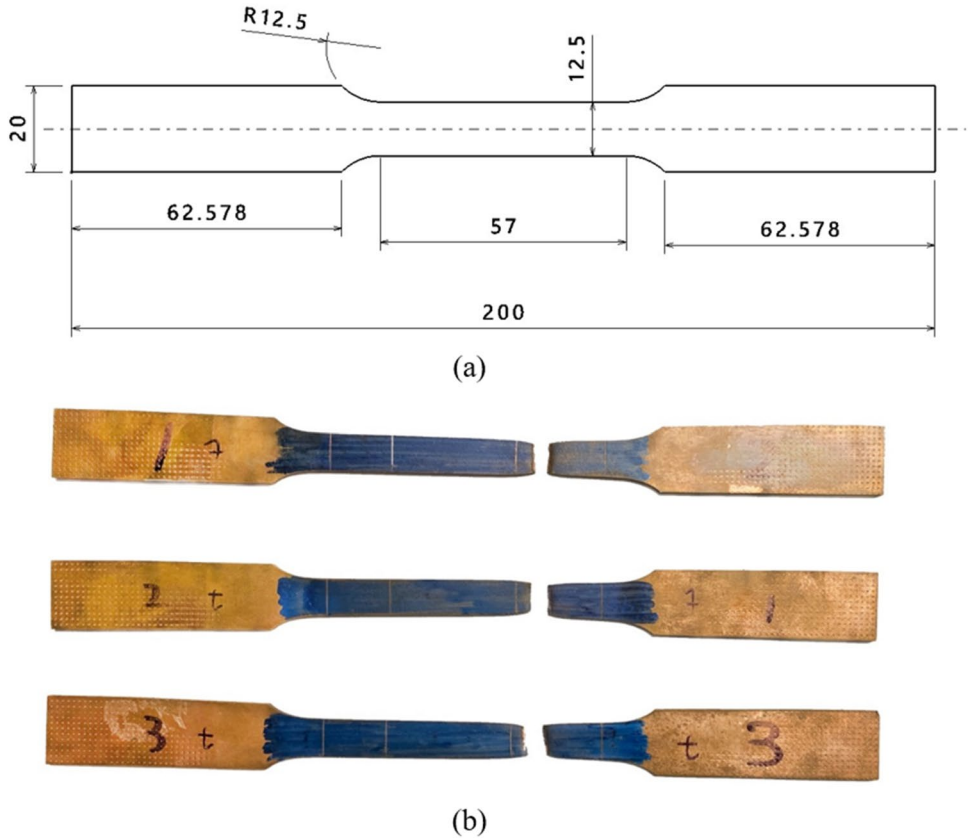

Fig. 5 **a** Size of the tensile test piece; **b** the tensile test piece

This study adopted Taguchi methods as the experimental design. These are systematic and effective methods that greatly reduce the number of experiments and can determine the optimal design parameter values that meet performance and cost requirements. The first step was to determine the key parameters. The most crucial fine-blanking process parameters that affect the fracture zone depth and die roll zone width in fine-blanking include the blanking velocity, V-ring height of the blank holder, V-ring height of the cavity, V-ring shape angle, V-ring position, blank holder force, counter punch force, and die clearance, which are illustrated in Fig. 11. In this experiment, the L_{18} ($2^1 \times 3^7$) orthogonal array was adopted. The process parameters and levels are explained as follows:

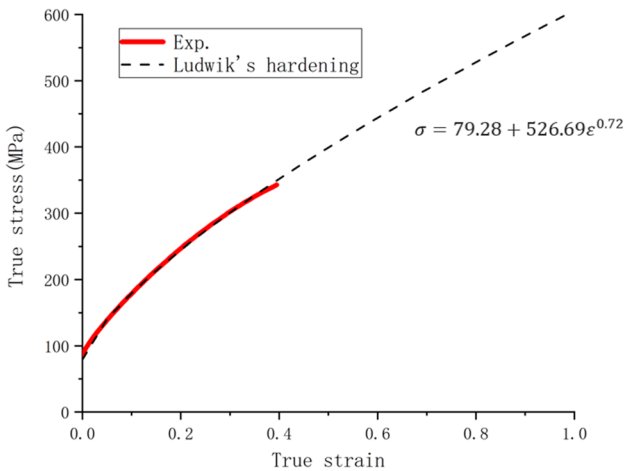

Fig. 6 True stress–true strain curve of C1100

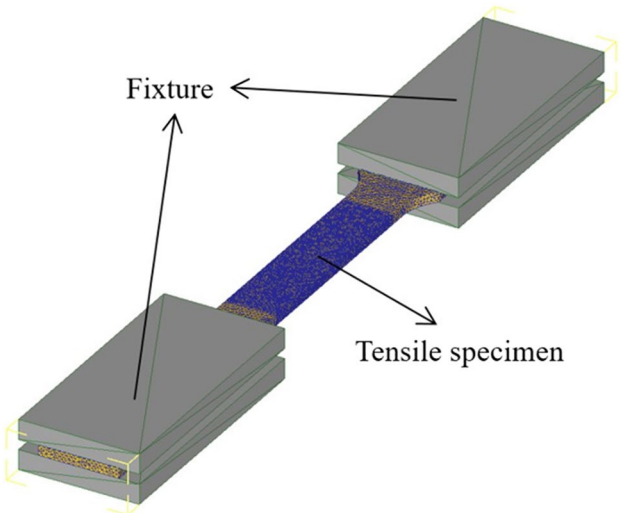

Fig. 7 Analysis model of the tensile test

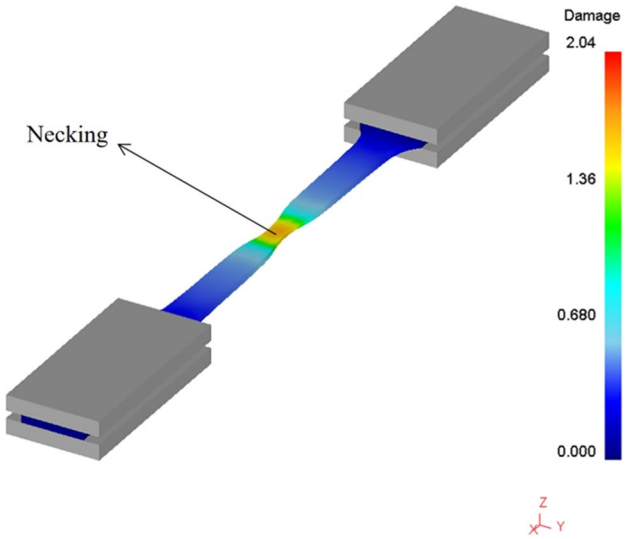

Fig. 8 Simulation result of the tensile test

(1) The height and position of the V-ring can affect the length of the shear zone. The precompression internal stress of the shear zone increases with the V-ring height, which increases the length of the shear zone. When the V-ring position is closer to the punch, the length of the shear zone increases, and the width and length of the die roll zone decrease [1]. Therefore, this study set three levels for each parameter: the heights of the V-ring on the blank holder were 0.1, 0.2, and 0.3 mm; the heights of the V-ring on the cavity were 0.15, 0.30, and 0.45 mm; the positions of the V-ring were 0.15, 0.20, and 0.25 mm; and the V-ring shape angles were 60, 90, and 120°.

(2) When the die clearance increases, the shear zone of the material is widely diffused, causing the blank to enter the fracture zone early during shearing, which in turn affects the depth of the shear zone [22]. In fine-blanking, the die clearance was approximately 0.5–1.5% of the blank thickness (2.5mm), and the die clearances were 0.0125, 0.025, and 0.0375 mm.

(3) Increases in blank holder force and counter punch force will cause the material flow to rotate in the shear zone, thus increasing the precompression internal stress to prevent cracks [23]. The blank holder forces selected were 100, 140, and 180 KN, while the counter punch forces were 80, 115, and 150 KN.

(4) Blanking velocity is strongly related to increasing production speed, which were slow speed 2 mm/s and fast speed 10 mm/s.

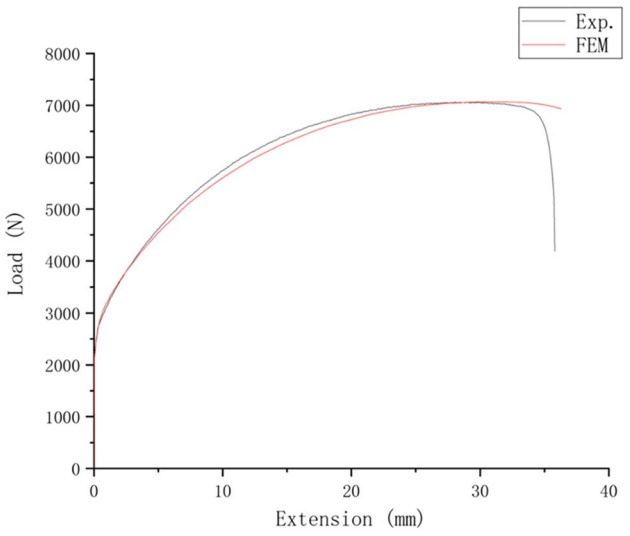

Fig. 9 Load–elongation values of the simulation analysis and the experimental results

The aforementioned experimental parameters and levels (as presented in Table 1) were configured for the L_{18} ($2^1 \times 3^7$) Taguchi orthogonal array, as presented in Table 2.

This study used DEFORM 2D to simulate the fine-blanking process and optimize the process parameters. The analysis model included the punch, blank holder, blank, counter punch, and cavity, as depicted in Fig. 12a. The CATIA software package was used to draw the geometry of the experimental die and import it into DEFORM-2D. The blank material was set as an elastoplastic body, while the punch, blank holder, cavity, and counter punch were set as a rigid body. Approximately 10,000 meshes were established on the blank, and local mesh refinement was performed in the shear and deformation zones. The size of the generated mesh was approximately 0.04×0.04 mm^2, and the friction coefficient was set to 0.12 according to T. S. Kwak et al. [23]. To prevent excessive deformation of the mesh or it penetrating into the die, the mesh was automatically refined when the interference was greater than 0.01 mm to prevent calculation divergence. The simulation process used an isotropic elastic–plastic material model to define the deformation behavior of the blank, the true stress–true strain curve obtained by the tensile test, and the critical damage value obtained by the tensile test simulation analysis, which were imported into the FEA software. The simulation was of the blanking process from the punch to the end position after the punch contacted the blank, as depicted in Fig. 12b.

To effectively determine the die roll zone width and fracture zone depth, the contour line of the shear cross-section by FEA results were converted into IGS files and imported into CATIA software. During the blanking process, the shear cross-section of the blank was divided into the fracture, shear, and die roll zones from top to bottom, as presented in Fig. 13. Therefore, the

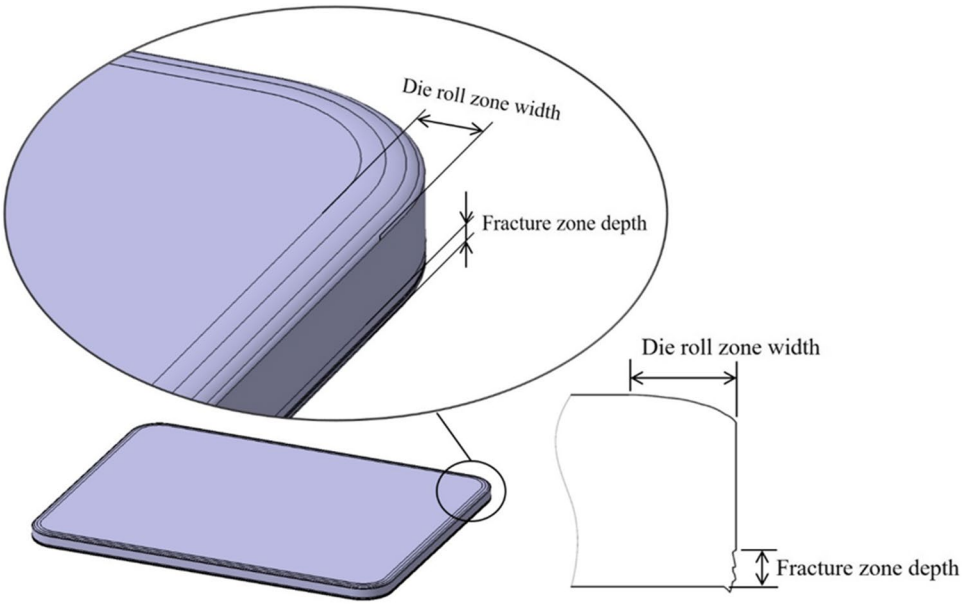

Fig. 10 Fracture zone depth and die roll zone width of the CPU thermal heat spreader, which were selected as the quality objectives

contour line of the shear cross-section above and below the shear zone was defined as the fracture zone and the die roll zone, respectively. The shearing surface of the blank was close to the cavity wall during the blanking process, and shearing zone was a vertical line $\overline{ab}$. The vertical distance from point a to point c (top side of the blank) is the fracture zone depth $\overline{ac}$. The vertical distance from point b to point d (bottom side of the blank) is the die roll zone depth $\overline{bd}$. The horizontal distance from point e (end point of the horizontal line on the bottom side) to the vertical line $\overline{ab}$ is the die roll zone width.

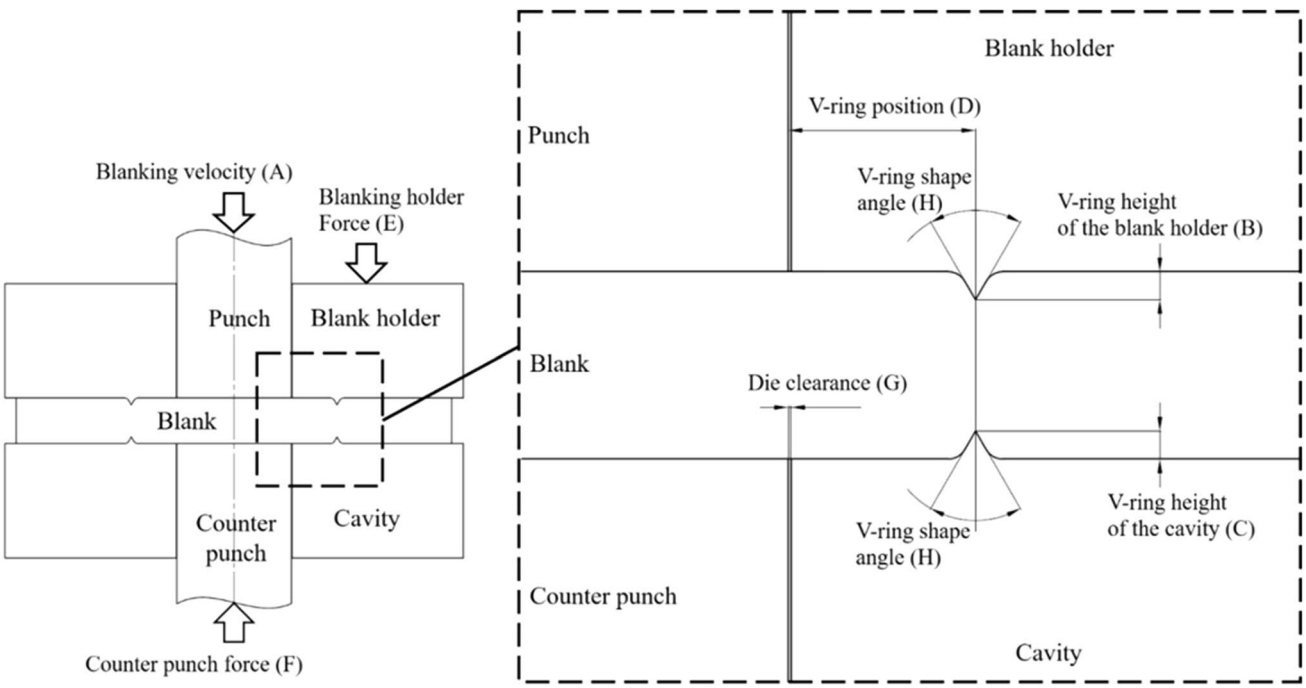

Fig. 11 Fine-blanking process parameters

Table 1 Level values for process parameters of fine-blanking

Parameters		Factor level		
		1	2	3
A	Blanking velocity (mm/s)	2	10	—
B	V-ring height of the blank holder (mm)	0.1	0.2	0.3
C	V-ring height of the cavity (mm)	0.15	0.3	0.45
D	V-ring position (mm)	1.5	2	2.5
E	Blanking holder force (N)	100000	140000	180000
F	Counter punch force (N)	80000	115000	150000
G	Die clearance (mm)	0.0125	0.025	0.0375
H	V-ring shape angle (°)	60	90	120

5 Results and discussion

5.1 Single-objective optimization

The Taguchi methods used the signal-to-noise (S/N) ratio for quality measurement. Through process parameter design experiments, the predictable part was used as the signal, and the unpredictable part was used as noise. In addition, the predictable part was maximized, and the unpredictable part was minimized to improve quality and reduce variation. In this study, the fracture zone depth and die roll zone width were selected as the quality objectives, and the fracture zone depth on the shear surface was reduced to improve the dimensional accuracy of the finished product. Furthermore, the die roll zone width was reduced to improve the heat dissipation efficiency. Therefore, both quality objectives adopted the smaller-the-better design. The S/N ratio calculation method was as follows:

$$S/N = 10\log_{10}(MSD) = -10\log_{10}\left(\frac{1}{n}\sum_{i=1}^{n} y_i^2\right) \quad (3)$$

The analysis data and S/N ratio are listed in Table 3, and an S/N ratio response graph using Taguchi methods is presented in Fig. 14. The optimal combination of process parameters with fracture zone depth as the quality objective consisted of a blanking velocity of 2 mm/s, blank holder V-ring height of 0.2 mm, cavity V-ring height of 0.45 mm, V-ring position of 2 mm, blank holder force of 180,000 N, counter punch force of 150,000 N, die clearance of 0.0125 mm, and V-ring shape angle of 60°. This combination was the fifth group of experiments in L18, and the fracture zone depth was 0.164 mm. Moreover, ANOVA was performed to calculate the degree of effect of each process parameter on the quality objectives. The results of quality variance analysis of the fracture zone depth are presented in Table 4, where counter punch force can be observed to have made the highest contribution (25.89%) to the fracture zone depth. This was followed by the V-ring position (21.02%), cavity V-ring height (19.03%), die clearance (11.13%), blank holder V-ring height (10.05%), blank holder force (6.72%), V-ring shape angle (3.41%), and lastly blanking velocity (0.25%).

Table 2 Parameter configuration of the L18 ($2^1 \times 3^7$) Taguchi orthogonal array

No.	Parameters							
	A (mm/s)	B (mm)	C (mm)	D (mm)	E (N)	F (N)	G (mm)	H (°)
1	2	0.1	0.15	1.5	100000	80000	0.0125	60
2	2	0.1	0.3	2	140000	115000	0.025	90
3	2	0.1	0.45	2.5	180000	150000	0.0375	120
4	2	0.2	0.15	1.5	140000	115000	0.0375	120
5	2	0.2	0.3	2	180000	150000	0.0125	60
6	2	0.2	0.45	2.5	100000	80000	0.025	90
7	2	0.3	0.15	2	100000	150000	0.025	120
8	2	0.3	0.3	2.5	140000	80000	0.0375	60
9	2	0.3	0.45	1.5	180000	115000	0.0125	90
10	10	0.1	0.15	2.5	180000	115000	0.025	60
11	10	0.1	0.3	1.5	100000	150000	0.0375	90
12	10	0.1	0.45	2	140000	80000	0.0125	120
13	10	0.2	0.15	2	180000	80000	0.0375	90
14	10	0.2	0.3	2.5	100000	115000	0.0125	120
15	10	0.2	0.45	1.5	140000	150000	0.025	60
16	10	0.3	0.15	2.5	140000	150000	0.0125	90
17	10	0.3	0.3	1.5	180000	80000	0.025	120
18	10	0.3	0.45	2	100000	115000	0.0375	60

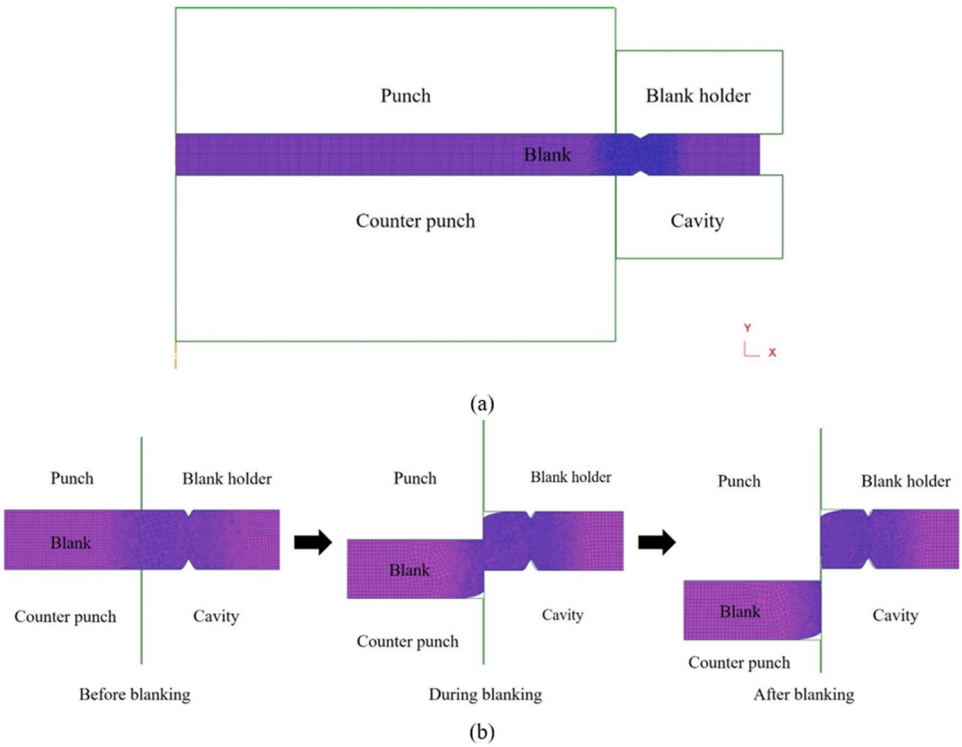

Fig. 12 **a** Analysis model of fine-blanking; **b** fine-blanking simulation process

In the results of the optimized analysis of the fracture zone depth, the precompression internal stress distribution diagram in the deformation zone of the workpiece when the V-ring is pressed into the sheet is shown in Fig. 15a. The material around the V-ring is compressed to produce a larger precompression internal stress of about 300MPa. As the distance from the V-ring gradually decreases, a larger precompression internal stress of about 113–150 MPa is

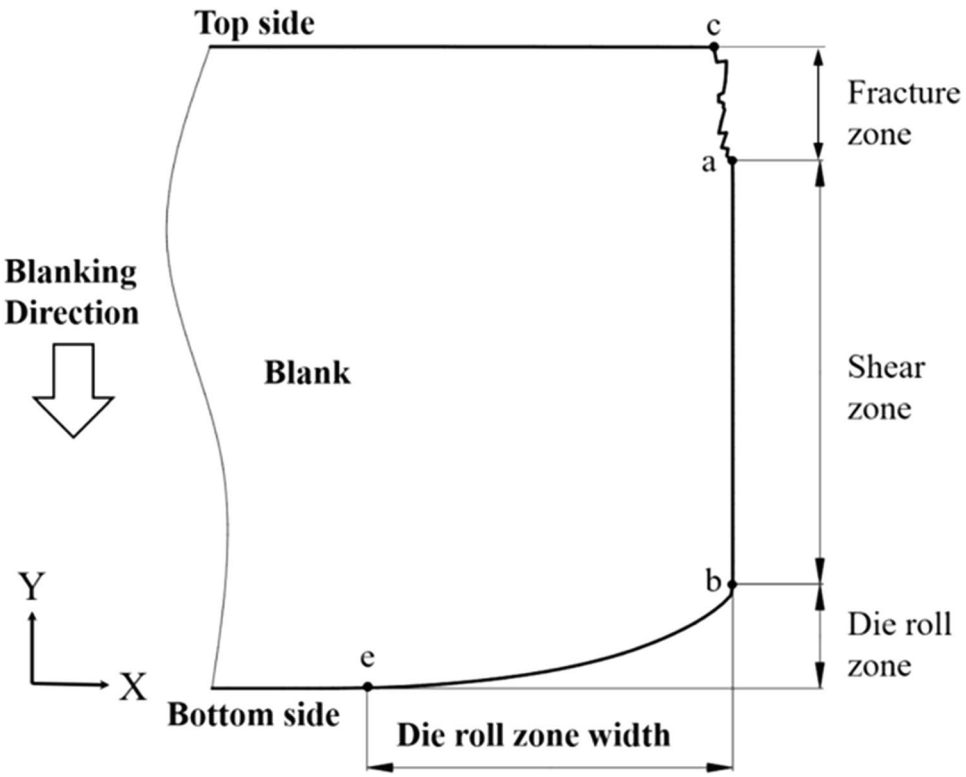

Fig. 13 Defining the areas in the shear cross-section

Table 3 L18 orthogonal array analysis results of fracture zone depth

No.	Parameters								Fracture zone depth (mm)	S/N(dB)
	A (mm/s)	B (mm)	C (mm)	D (mm)	E (N)	F (N)	G (mm)	H (°)		
1	2	0.1	0.15	1.5	100000	80000	0.0125	60	1.092	−0.7645
2	2	0.1	0.3	2	140000	115000	0.025	90	0.591	4.5653
3	2	0.1	0.45	2.5	180000	150000	0.0375	120	0.444	7.0465
4	2	0.2	0.15	1.5	140000	115000	0.0375	120	0.724	2.8028
5	2	0.2	0.3	2	180000	150000	0.0125	60	0.164	15.6820
6	2	0.2	0.45	2.5	100000	80000	0.025	90	0.733	2.6956
7	2	0.3	0.15	2	100000	150000	0.025	120	0.660	3.6118
8	2	0.3	0.3	2.5	140000	80000	0.0375	60	0.502	5.9911
9	2	0.3	0.45	1.5	180000	115000	0.0125	90	0.697	3.1391
10	10	0.1	0.15	2.5	180000	115000	0.025	60	0.884	1.0729
11	10	0.1	0.3	1.5	100000	150000	0.0375	90	0.612	4.2650
12	10	0.1	0.45	2	140000	80000	0.0125	120	0.517	5.7335
13	10	0.2	0.15	2	180000	80000	0.0375	90	0.606	4.3491
14	10	0.2	0.3	2.5	100000	115000	0.0125	120	0.507	5.8947
15	10	0.2	0.45	1.5	140000	150000	0.025	60	0.500	6.0171
16	10	0.3	0.15	2.5	140000	150000	0.0125	90	0.478	6.4151
17	10	0.3	0.3	1.5	180000	80000	0.025	120	0.784	2.1170
18	10	0.3	0.45	2	100000	115000	0.0375	60	0.504	5.9531

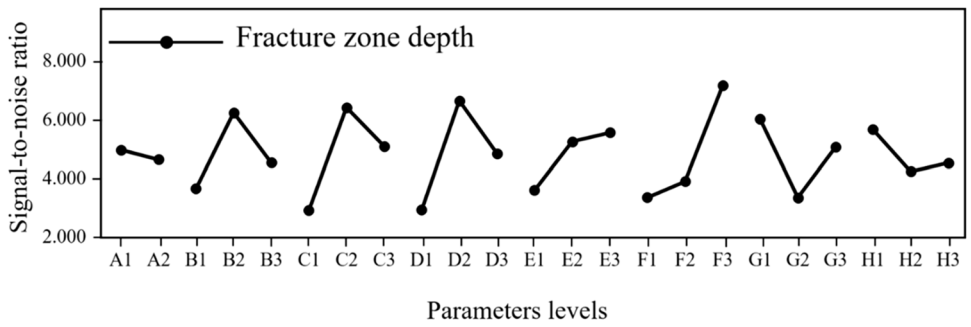

Fig. 14 S/N ratio response graph of fracture zone depth

Table 4 ANOVA results for fracture zone depth

Parameters	Degree of freedom	Sum of squares	Variance	Net sum of squares	*F* test	Contribution (%)
A. Blanking velocity (mm/s)	1	0.484	0.484	−3.580	0.238	0.25
B. V-ring height of the blank holder (mm)	2	20.748	10.374	12.619	5.105	10.5
C. V-ring height of the cavity (mm)	2	37.589	18.795	29.461	9.249	19.03
D. V-ring position (mm)	2	41.525	20.762	33.396	10.217	21.02
E. Blank holder force (N)	2	13.279	6.640	5.151	3.267	6.72
F. Counter punch force (N)	2	51.143	25.572	43.015	12.584	25.89
G. Die clearance (mm)	2	21.984	10.992	13.856	5.409	11.13
H. V-ring shape angle (°)	2	6.739	3.369	−1.390	1.658	3.41
Standard deviation	2	4.064	2.032	−4.064		2.06
Sum	17	197.555				100%

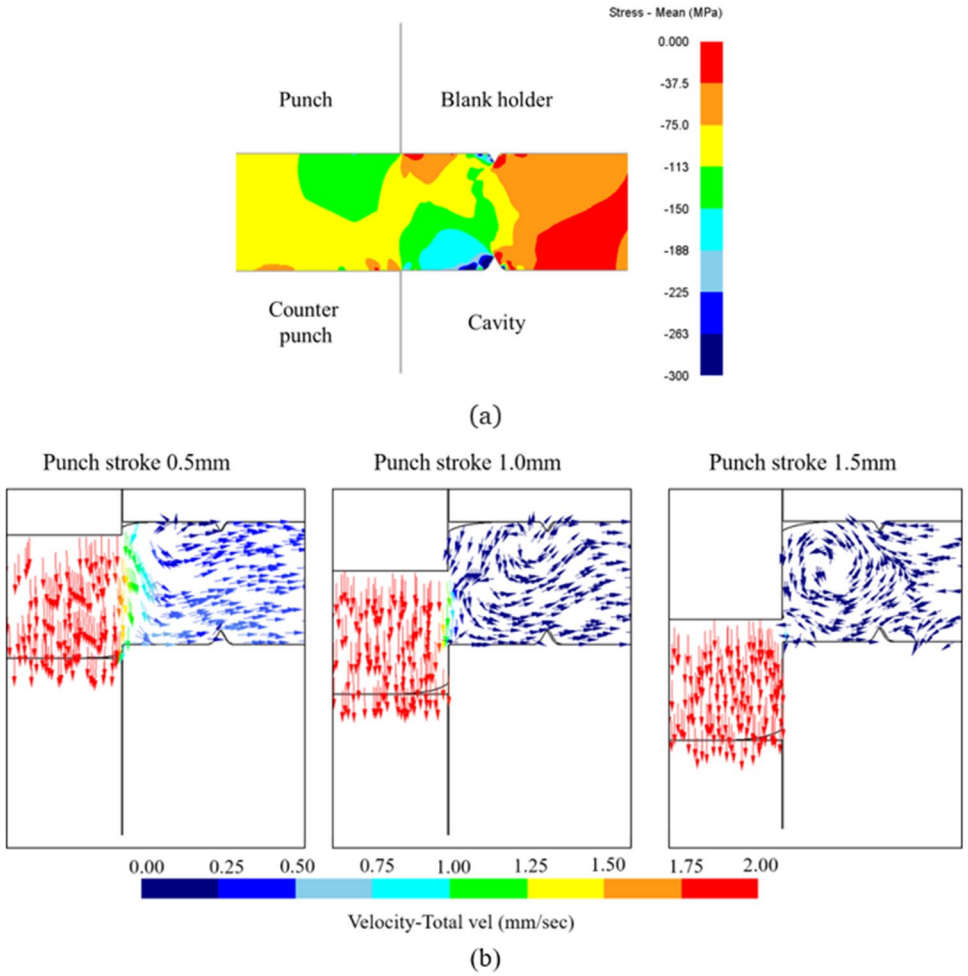

Fig. 15 The optimal of fracture zone depth: **a** the stress distribution on workpiece before the blanking phase; **b** the material flow analysis during the blanking phase

generated in the blanking area, which effectively suppress the occurrence of fracture zone in the fine-blanking process. With a punch stroke of 1.0 mm, the rotation of the material flow became gradually closely the V-ring shape, as shown in Fig. 15b. With a punch stroke of 1.5 mm, the material is about to separate. The material flow continues rotating closely the V-ring shape, to prevent the material flowing into the shear zone and to reduce the fracture zone depth.

When the die roll zone width was the quality objective, measurements were performed using the smaller-the-better design. According to the analysis results of the L_{18} orthogonal array (Table 5) and the S/N ratio response graph (Fig. 16), the optimized parameter combination for die roll zone width was a blanking velocity of 10 mm/s, blank holder V-ring height of 0.2 mm, cavity V-ring height of 0.45 mm, V-ring position of 1.5 mm, blank holder force of 140,000 N, counter punch force of 150,000 N, die clearance of 0.0125 mm, and V-ring shape angle of 90°. The die roll zone width was 1.274 mm, which was a reduction of 0.034 mm from the smallest die roll zone width in L18. The quality ANOVA results for the die roll zone width are presented in Table 6, where the V-ring height of the cavity (29.45%) can be observed to have made the highest contribution. This was followed by the V-ring shape angle (28.88%), die clearance (25.54%), V-ring height of the blank holder (4.70%), V-ring position (3.91%), blanking velocity (3.69%), counter punch force (2.40%), and blank holder force (1.13%).

In the results of the optimized analysis of the die roll zone, the precompression internal stress distribution diagram in the deformation zone of the workpiece when the V-ring is pressed into the sheet is shown in Fig. 17a. The material around the V-ring is compressed to produce a larger precompression internal stress of about 300 MPa. As the distance from the V-ring gradually decreases, a larger precompression internal stress of about 75–150 MPa is generated in the blanking area. However, a relatively large precompression internal stress of about 225 MPa is generated between the counter punch and the cavity, so the material can resist the compressive stress in the initial stage of fine-blanking process, to reduce the die roll zone width. With a punch stroke of 1.0 mm, the rotation of the material flow became gradually closely the V-ring shape, as shown in Fig. 17b. With a punch stroke of 1.5 mm, the material is about to separate. The V-ring cannot effectively prevent the material

Table 5 L18 orthogonal array analysis results of die roll zone width

No.	Parameters								Roll zone width (mm)	S/N(dB)
	A (mm/s)	B (mm)	C (mm)	D (mm)	E (N)	F (N)	G (mm)	H (°)		
1	2	0.1	0.15	1.5	100000	80000	0.0125	60	1.522	−3.646
2	2	0.1	0.3	2	140000	115000	0.025	90	1.478	−3.395
3	2	0.1	0.45	2.5	180000	150000	0.0375	120	1.608	−4.127
4	2	0.2	0.15	1.5	140000	115000	0.0375	120	1.686	−4.536
5	2	0.2	0.3	2	180000	150000	0.0125	60	1.376	−2.771
6	2	0.2	0.45	2.5	100000	80000	0.025	90	1.415	−3.012
7	2	0.3	0.15	2	100000	150000	0.025	120	1.798	−5.096
8	2	0.3	0.3	2.5	140000	80000	0.0375	60	1.597	−4.064
9	2	0.3	0.45	1.5	180000	115000	0.0125	90	1.323	−2.429
10	10	0.1	0.15	2.5	180000	115000	0.025	60	1.560	−3.862
11	10	0.1	0.3	1.5	100000	150000	0.0375	90	1.462	−3.297
12	10	0.1	0.45	2	140000	80000	0.0125	120	1.476	−3.380
13	10	0.2	0.15	2	180000	80000	0.0375	90	1.599	−4.077
14	10	0.2	0.3	2.5	100000	115000	0.0125	120	1.456	−3.262
15	10	0.2	0.45	1.5	140000	150000	0.025	60	1.309	−2.337
16	10	0.3	0.15	2.5	140000	150000	0.0125	90	1.415	−3.013
17	10	0.3	0.3	1.5	180000	80000	0.025	120	1.578	−3.961
18	10	0.3	0.45	2	100000	115000	0.0375	60	1.495	−3.492

from entering the shear zone. At this time, the material flow direction is omnidirectional to the shearing area.

5.2 Multicriteria optimization

According to a comparison of optimized combination results between the fracture zone depth and die roll zone width (Table 7), both zones were in conflict with some parameter levels, making it difficult to select the optimal parameter level for multiple objectives. Therefore, this study adopted the method of Kunjur and Krishnamurty to extend the Taguchi method and developed a robust multicriteria optimal approach [24] to discuss the level combination of multiobjective optimal process parameters.

(1) Parameter A (blank velocity): the contribution of blank velocity was 0.25% and 3.69% to the fraction zone depth and die roll zone width, respectively. These contributions were both low. However, an *F* test on the die roll zone width was $F_A > F_{0.05}(2, 2) = 19$, making blank velocity a significant parameter to the die roll zone width. Therefore, 10 mm/s was selected as the optimal level with high production efficiency.

(2) Parameter B (V-ring height of the blank): this parameter's contribution to the fraction zone depth and die roll zone width was 10.50% and 4.70%, respectively, which were determined to be low contributions to both zones. However, once this parameter was optimized in both objectives through single-objective optimization, 0.2 mm was selected as the optimal level.

(3) Parameter C (V-ring height of the cavity): this parameter's contribution to the fraction zone depth and die roll zone width was 19.03% and 29.45%, respectively, which were determined to be medium contributions to both zones. Nevertheless, the *F* test result of the die roll

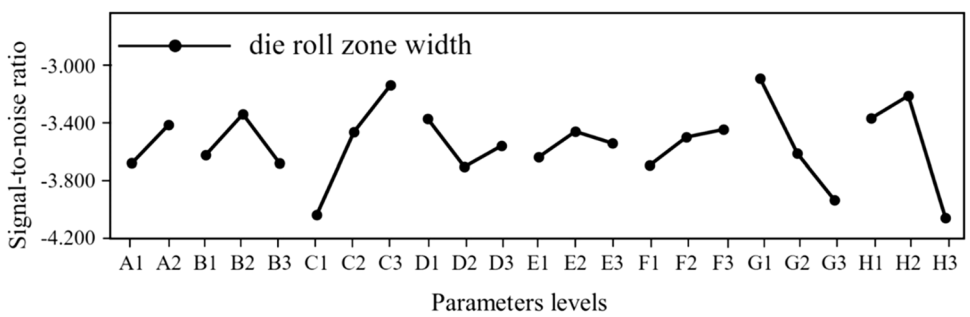

Fig. 16 S/N ratio response graph of die roll zone width

Table 6 ANOVA results for die roll zone width

Parameters	Degree of freedom	Sum of squares	Variance	Net sum of squares	*F* test	Contribution (%)
A. Blanking velocity (mm/s)	1	0.319	0.319	0.292	24.165	3.69%
B. V-ring height of the blank holder (mm)	2	0.406	0.203	0.353	15.374	4.70%
C. V-ring height of the cavity (mm)	2	2.541	1.270	2.488	96.312	29.45%
D. V-ring position (mm)	2	0.337	0.169	0.284	12.776	3.91%
E. Blank holder force (N)	2	0.098	0.049	0.045	3.699	1.13%
F. Counter punch force (N)	2	0.207	0.103	0.154	7.839	2.40%
G. Die clearance (mm)	2	2.203	1.102	2.151	83.526	25.54%
H. V-ring shape angle (°)	2	2.491	1.246	2.438	94.440	28.88%
Standard deviation	2	0.026	0.013	−0.026		0.31%
Sum	17	8.627				100%

zone width was $F_C > F_{0.05}(2, 2) = 19$. Thus, this parameter was determined to be significant to the die roll zone width, and 0.45 mm was selected as the optimal level.

(4) Parameter D (V-ring position): this parameter's contribution to the fracture zone depth was a moderate 21.02%, and its contribution to the die roll zone width was low at 3.91%. Therefore, it was determined to be a secondary parameter, and the original design interval was used as the adjustment interval.

(5) Parameter E (blank holder force): this parameter's contribution was 6.72% and 1.13% to the fraction zone depth and die roll zone width, respectively. The

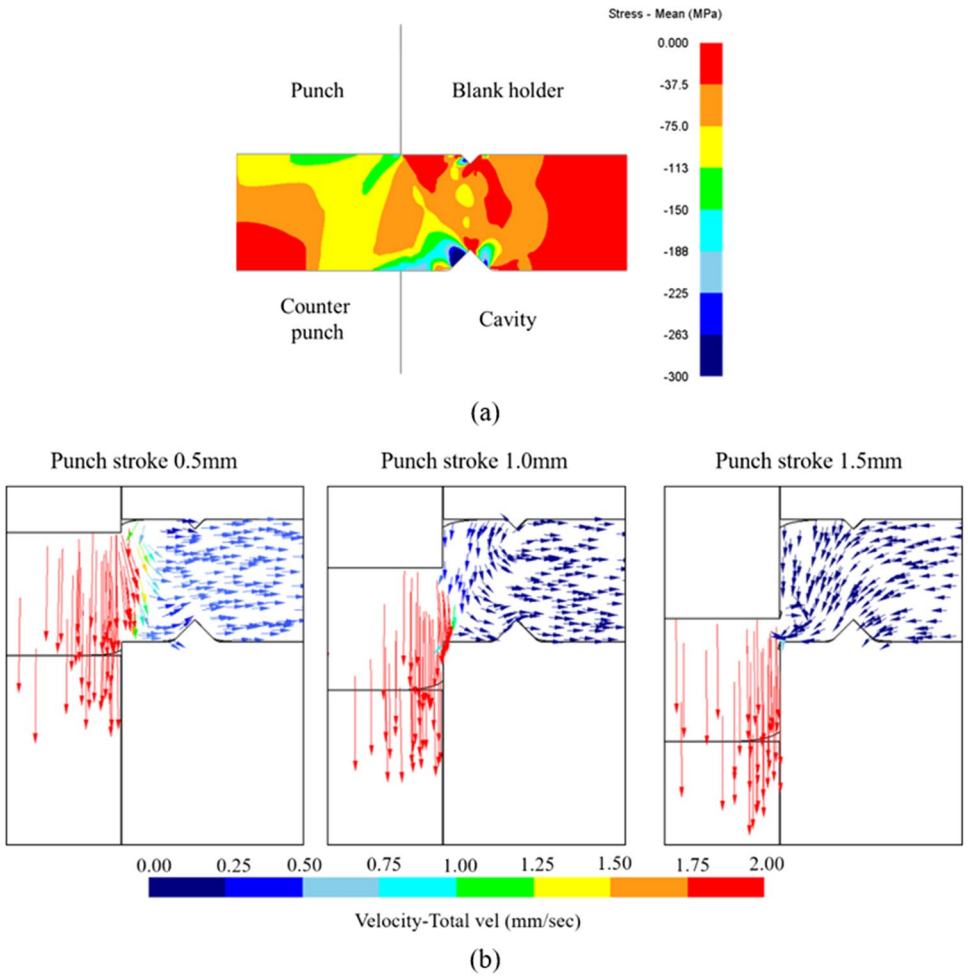

Fig. 17 The optimal of die roll zone width: **a** the stress distribution on workpiece before the blanking phase; **b** the material flow analysis during the blanking phase

Table 7 Comparison of optimization results between fracture zone depth and die roll zone width

Selected quality objectives for optimization	Parameters								Fracture zone depth (mm)	Die roll zone width (mm)
	A (mm/s)	B (mm)	C (mm)	D (mm)	E (N)	F (N)	G (mm)	H (°)		
Fracture zone depth	2	0.2	0.3	2	180000	150000	0.0125	60	0.164	1.376
Die roll zone width	10	0.2	0.45	1.5	140000	150000	0.0125	90	0.512	1.274

parameter was nonsignificant because both contributions were low and the F test result of the two was less than $F_{0.05}(2, 2) = 19$. To ensure the blank had greater precompression internal stress, 180,000 N was selected as the optimal level.

(6) Parameter F (counter punch force): this parameter's contribution to the fracture zone depth was a moderate 25.89%, and its contribution to the die roll zone width was low at 2.40%. This parameter was determined to be a secondary parameter, and the original design interval was used as the adjustment interval.

(7) Parameter G (die clearance): this parameter's contribution was 11.13% and 25.54% to the fraction zone depth and die roll zone width, respectively. In addition, the F test result of the die roll zone width was $F_G > F_{0.05}(2, 2) = 19$, which demonstrated that this parameter was significant to the die roll zone width. Therefore, 0.0125 mm was selected as the optimal level.

(8) Parameter H (V-ring shape angle): this parameter's contribution was 3.41% and 28.88% to the fraction zone depth and die roll zone width, respectively. Moreover, the F test result of the die roll zone width was $F_H > F_{0.05}(2, 2) = 19$; therefore, the parameter was significant to die roll zone width, and 90° was selected as the optimal level.

The process parameter range of the robust multicriteria optimal approach is as follows:

$A = 10$ mm/s, $B = 0.2$ mm, $C = 0.45$ mm, 1.5 mm $\leq D \leq$ 2.5 mm, $E = 180{,}000$ N, 80,000 mm $\leq F \leq$ 150,000 mm, $G = 0.0125$ mm, $H = 90°$

According to the aforementioned design range, a set of Pareto-optimal solutions was generated for a simulation analysis [24]. Table 8 presents the Pareto optimality simulation results. In compliance with the industry standard, the fraction zone depth had to be less than 12% (0.3 mm) of the blank thickness, which is the main consideration, and the die roll zone width is the secondary consideration. The second set of simulation results, presented in Table 8 and Fig. 18, obtained the smallest fraction zone depth. It ranked second in die roll zone width, which was only 0.008 mm away from the first. Therefore, the following parameters were selected as the robust multicriteria optimal process parameter combination: blanking velocity of 10 mm/s, blank holder V-ring height of 0.2 mm, cavity V-ring height of 0.45 mm, V-ring position of 2 mm, blank holder force of 180,000 N, counter punch force of 115,000 N, die clearance of 0.0125 mm, and V-ring shape angle of 90°.

Table 8 Pareto-optimal solution analysis results of fine-blanking parameters

No.	Parameters								Fracture zone width (mm)	Die roll zone width (mm)
	A (mm/s)	B (mm)	C (mm)	D (mm)	E (N)	F (N)	G (mm)	H (°)		
1	10	0.2	0.45	1.5	180000	80000	0.0125	90	0.518	1.396
2	10	0.2	0.45	2	180000	115000	0.0125	90	0.239	1.288
3	10	0.2	0.45	2.5	180000	150000	0.0125	90	0.559	1.345
4	10	0.2	0.45	1.5	180000	115000	0.0125	90	0.544	1.293
5	10	0.2	0.45	2	180000	150000	0.0125	90	0.324	1.280
6	10	0.2	0.45	2.5	180000	80000	0.0125	90	0.257	1.373
7	10	0.2	0.45	1.5	180000	150000	0.0125	90	0.530	1.280
8	10	0.2	0.45	2	180000	80000	0.0125	90	0.473	1.342
9	10	0.2	0.45	2.5	180000	115000	0.0125	90	0.396	1.334

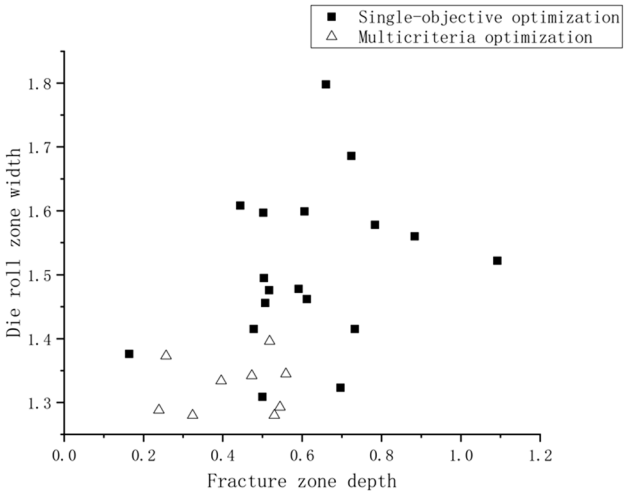

Fig. 18 Pareto-optimal solutions for the fine-blanking parameters

5.3 Experiment and verification

To confirm the accuracy of the FEA software, experiments were conducted to verify the analysis results. The robust multicriteria optimal process parameter combination was used to conduct a forming experiment, and the measurement results of the fracture zone depth and die roll zone width were compared with the analysis results. Figure 19 depicts the finished product and measurement position of the fine-blanking experiment. A comparison between the experimental and analytical results is presented in Table 9. In terms of fraction zone depth, the analytical value of the model was 0.009 mm larger than the experimental value, which was considered consistent. In terms of die roll zone width, although the FEA set the blank as an isotropic material, the blank became an anisotropic material after being processed by rolling. Therefore, when the blank crystallite rolling direction was perpendicular to the die cavity edge (A zone in Fig. 19), the die roll zone width of 1.109 mm outperformed the simulation result. In addition, when the blank crystallite rolling direction was parallel to the die cavity edge (B zone in Fig. 19), the die roll zone width was 1.205 mm, which was less than the simulation result of 1.288 mm, but both values were close. The shear cross-section of the product was measured using a three-dimensional laser scanning confocal microscope (VK-X100 K, Keyence Inc., Japan) to scan the surface topography of the fine-blanking shear surface (A Zone). The results are presented in Fig. 20.

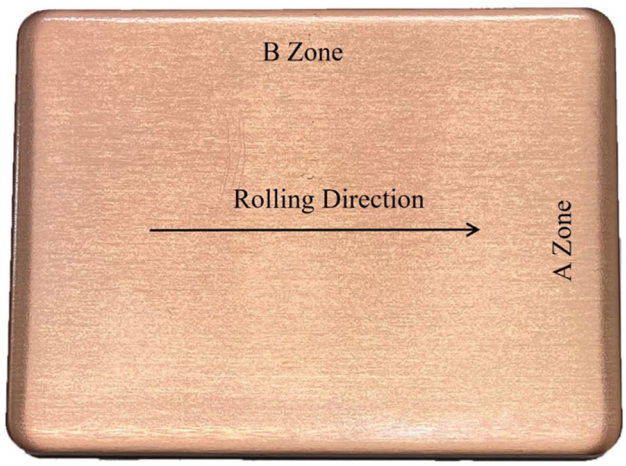

Fig. 19 Measuring position of the CPU thermal heat spreader

Table 9 Comparison of experimental and analytical results

Value	Fracture zone depth (mm)	Die roll zone width (mm)	
		A Zone	B Zone
Experimental value-1	0.214	1.258	1.234
Experimental value-2	0.227	0.928	1.313
Experimental value-3	0.236	1.036	1.071
Experimental value-4	0.243	1.216	1.203
Experimental Mean	0.230	1.109	1.205
Analytical value	0.239	1.288	

6 Conclusion

In this study, the fine-blanking of a CPU thermal heat spreader was used as an example to optimize the process parameters. To reduce the fracture zone depth and die roll zone width, single-objective optimization of the fine-blanking parameters was performed. Subsequently, the effect of the fine-blanking parameters on each quality objective for robust multicriteria optimal design was analyzed, and the optimal design results were verified with experiments. The research results can be summarized as follows:

(1) Taking the fracture zone depth as the quality objective, the optimal combination of process parameters was a blanking velocity of 2 mm/s, blank holder V-ring height of 0.2 mm, cavity V-ring height of 0.45 mm, V-ring position of 2 mm, blank holder force of 180,000 N, counter punch force of 150,000 N, die clearance of 0.0125 mm, and V-ring shape angle of 60°. The fracture zone depth was 0.164 mm. According to the ANOVA results, the effect of the counter punch force was the largest with a contribution of 25.89%. The frac-

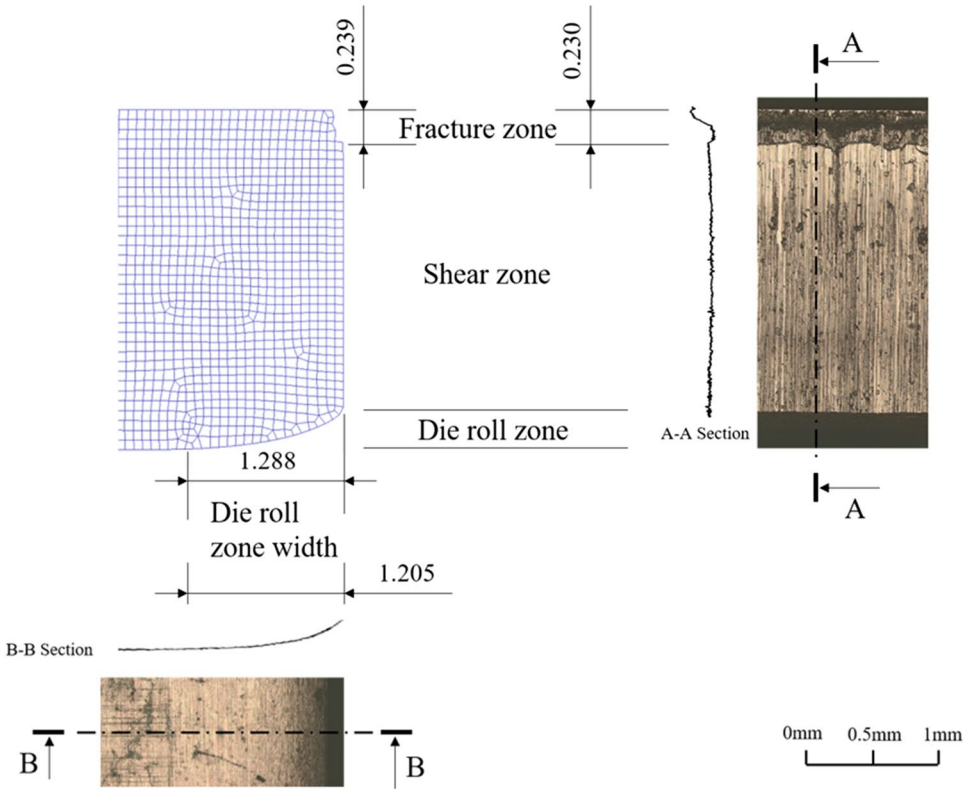

Fig. 20 Shear cross-section of fine-blanking (A Zone)

ture zone depth decreased as the counter punch force tonnage became higher.

(2) Taking die roll zone width as the quality objective, the optimal combination of process parameters was a blanking velocity of 10 mm/s, blank holder V-ring height of 0.2 mm, cavity V-ring height of 0.45 mm, V-ring position of 1.5 mm, blank holder force of 140,000 N, counter punch force of 150,000 N, die clearance of 0.0125 mm, and V-ring shape angle of 90°. The die roll zone width was 1.274 mm. In addition, the ANOVA results indicated that the effect of the V-ring height of the cavity was the largest with a contribution of 29.45%. Increasing the V-ring height of the cavity will reduce the die roll zone width accordingly.

(3) This study used a robust multicriteria optimal approach and Pareto-optimal solutions and set the fracture zone depth as the main objective and the die roll zone width as the secondary objective. The combination of multicriteria optimal process parameters was a blanking velocity of 10 mm/s, blank holder V-ring height of 0.2 mm, cavity V-ring height of 0.45 mm, V-ring position of 2 mm, blank holder force of 180,000 N, counter punch force of 115,000 N, die clearance of 0.0125 mm, and V-ring shape angle of 90°. This combination not only met the industry's standard for fracture zone depth but could also obtain a smaller die roll zone width.

(4) The comparison between the experimental and analysis results revealed that the difference in fracture zone depth was as small as 0.009 mm. In terms of die roll zone width, due to the blank grain rolling direction, the experimental result was 0.179 mm smaller than the analysis result when the cutting edge was perpendicular to the rolling direction. In addition, the experimental result was 0.083 mm smaller than the analysis result when the cutting edge was parallel to the rolling direction.

Author contribution The authors' contributions are as follows: all authors conceived and designed the study; Tse-Chang Li, Kuo-Wang Liu, and Dai-You Wu performed the theoretical deduction, performed the experiments and the finite element simulations, and performed the process optimization and analysis; and Chun-Chih Kuo and Tse-Chang Li contributed to the interpretation of the results. Kuo-Wang Liu and Dai-You Wu took the lead in writing the manuscript; Chun-Chih Kuo, Kuo-Wang Liu, and Bor-Tsuen Lin contributed actively in writing the manuscript; all authors provided critical feedback and helped shape the research, analysis, and manuscript.

Funding This work was financially supported by the Frontier Mould and Die Research and Development Center from The Featured Areas Research Center Program within the framework of the Higher Education Sprout Project by the Ministry of Education (MOE) in Taiwan.

Data availability The datasets generated during and/or analyzed during the current study are available from the corresponding author on reasonable request.

Declarations

Ethics approval The authors claim that none of the contents in this manuscript has been published or considered for publication elsewhere. Besides, the research contents of the article do not violate ethics.

Consent to participate This manuscript does not involve human or animal participation or data; therefore, consent to participate is not applicable.

Consent for publication This manuscript does not contain data from any individual person; therefore, consent to publish is not applicable.

Competing interests The authors declare no competing interests.

References

1. Thipprakmas S (2010) Application of Taguchi technique to investigation of geometry and position of V-ring indenter in fine-blanking process. Mater Design 31:2496–2500
2. Yin F, Mao H, Hua L, Gu Z (2012) Back propagation neural network based calculation model for predicting wear of fine-blanking die during its whole lifetime. Computational Mater Sci 59:140–151
3. Liu Y, Hua L, Mao H, Feng W (2014) Finite element simulation of effect of part shape on forming quality in fine-blanking process. Procedia Eng 81:1108–1113
4. Wang J-P (2015) A novel fine-blanking approach. Int J Advanced Manufact Technol 78:1015–1019
5. Liu Y, Tang B, Hua L, Mao H (2018) Investigation of a novel modified die design for fine-blanking process to reduce the die-roll size. J Mater Process Technol 260:30–37
6. Zheng Q, Zhuang X, Zhao Z (2019) State-of-the-art and future challenge in fine-blanking technology. Production Eng 13:61–70
7. Karnaukh SG, Markov OE, Aliieva LI, Kukhar VV (2020) Designing and researching of the equipment for cutting by breaking of rolled stock. Int J Advanced Manufact Technol 109:2457–2464
8. Sahli M, Roizard X, Assoul M, Colas G, Giampiccolo S, Barbe JP (2021) Finite element simulation and experimental investigation of the effect of clearance on the forming quality in the fine blanking process. Microsyst Technol 27:871–881
9. Hu XH, Choi KS, Sun X, Golovashchenko SF (2014) Edge fracture prediction of traditional and advanced trimming processes for AA6111-T4 sheets. J Manufact Sci Eng 136:021016 (11 pages)
10. Huang G, Wang J, Hsu M, Huang K, Chen T, Chen T (2017) Application of mold trough design to blanking technology. Int J Advanced Manufact Technol 88:1025–1034
11. Zhao PJ, Chen ZH, Dong CF (2016) Experimental and numerical analysis of micromechanical damage for DP600 steel in fine-blanking process. J Mater Process Technol 236:16–25
12. Wang S, Chen Z, Dong C (2017) Tearing failure of ultra-thin sheet-metal involving size effect in blanking process: analysis based on modified GTN model. Int J Mech Sci 133:288–302
13. Barik J, Sonkamble V, Narasimhan K (2018) Burr formation and shear strain field evolution studies during sheet metal blanking. IOP Conference Series: Mater Sci Eng 418:012068 (8 pages)
14. Tanaka T, Hagihara S, Tadano Y, Inada T, Mori T, Fuchiwaki K (2013) Application of finite element method to analysis of ductile fracture criteria for punched cutting surfaces. Mater Trans 54:1697–1702
15. Osakada K, Mori K, Altan T, Groche P (2011) Mechanical servo press technology for metal forming. CIRP Annals - Manufact Technol 60:651–672
16. Kriechenbauer S, Mauermann R, Muller P (2014) Deep drawing with superimposed low-frequency vibrations on servo-screw presses. Procedia Eng 81:905–913
17. Haase OC, Silveira VL, Stemler PM, Viana RA, Duarte AS (2018) Enabling stamping processes through meticulous FE modelling-segmented drawbeads and remesh criteria. IOP Conference Series: Mater Sci Eng 418:012091 (9 pages)
18. Kim S, Tsuruoka K, Yamamoto T (2014) Effect of forming speed in precision forging process evaluated using CAE technology and high performance servo-press machine. Procedia Eng 81:2415–2420
19. Olguner S, Bozdana AT (2017) Influence of press ram pulsation on deep drawability of dual phase steel sheet. Acta Physica Polonica A 132:742–745
20. Fallahiarezoodar A, Gupta T, Goertemiller C, Altan T (2019) Residual stresses and springback reduction in U-channel drawing of Al5182-O by using a servo press and a servo hydraulic cushion. Production Eng 13:219–226
21. Esmaeilpour R, Tiji SAN, Kim H, Park T, Kim H, Pourboghrat F, Mohammed B (2019) Stamping of a cross-shaped part with 5052, 5754 and 6016 aluminum alloy sheets–experimental and finite element analysis comparison. IOP Conference Series: Mater Sci Eng 521:012002 (6 pages)
22. Thipprakmas S, Jin M, Murakawa M (2007) An investigation of material flow analysis in fine-blanking process. J Mater Process Technol 192-193:237–242
23. Kwak TS, Kim YJ, Bae WB (2002) Finite element analysis on the effect of die clearance on shear planes in fine blanking. J Mater Process Technol 130-131:462–468
24. Kunjur A, Krishnamurty S (1997) A robust multi-criteria optimization approach. Mechanism Machine Theory 32:797–810
25. Sermpong N, Nuttakorn SE, Yingyo AUL (2018) Determination and analysis of critical damage criteria for predicting fracture in forming process by uniaxial tensile test. Mater Today: Proc 5:9642–9650
26. Joun M, Kim M, Kim J, Chung W (2014) Finite element analysis of deep piercing process. Procedia Eng 81:2494–2498
27. Fan WF, Li JH (2009) An investigation on the damage of AISI-1045 and AISI-1025 steels in fine-blanking with negative clearance. Mater Sci Engineering: A 499:248–251